Vadose-Zone Alteration of Metaschoepite and Ceramic UO2 in Savannah River Site Field Lysimeters

Fallon, Connaugh M.

2022-12-12

Fallon , C M , Bower , W , Powell , B , Livens , F R , Lyon , I C , McNulty , A , Peruski , K , Mosselmans , F , Kaplan , D , Grolimund , D , Warnicke , P , Ferreira-Sanchez , D , Sitar-Kauppi , M , Vettese , G , Shaw , S , Morris , K & Law , G 2022 , ' Vadose-Zone Alteration of Metaschoepite and Ceramic UO2 in Savannah River Site Field Lysimeters ' , The Science of the Total Environment , vol. 862 . https://doi.org/10.1016/j.scitotenv.2022.160862

http://hdl.handle.net/10138/355901
https://doi.org/10.1016/j.scitotenv.2022.160862

Science of the Total Environment 862 (2023) 160862

Contents lists available at ScienceDirect

Science of the Total Environment

journal homepage: www.elsevier.com/locate/scitotenv

Vadose-zone alteration of metaschoepite and ceramic UO_2 in Savannah River Site field lysimeters

Connaugh M. Fallon [a,b], William R. Bower [a,c], Brian A. Powell [d], Francis R. Livens [a,b], Ian C. Lyon [b], Alana E. McNulty [b], Kathryn Peruski [d], J. Frederick W. Mosselmans [e], Daniel I. Kaplan [f], Daniel Grolimund [g], Peter Warnicke [g], Dario Ferreira-Sanchez [g], Marja Siitari Kauppi [c], Gianni F. Vettese [c], Samuel Shaw [b], Katherine Morris [b], Gareth T.W. Law [c,*]

[a] Centre for Radiochemistry Research, Department of Chemistry, The University of Manchester, Manchester M13 9PL, UK,
[b] Research Centre for Radwaste and Decommissioning and Williamson Research Centre, Department of Earth and Environmental Sciences, The University of Manchester, Manchester M13 9PL, UK
[c] Radiochemistry Unit, Department of Chemistry, University of Helsinki, Helsinki 00014, Finland
[d] Department of Environmental Engineering and Earth Sciences, Department of Chemistry, Clemson University, Clemson, SC 29634, USA
[e] Diamond Light Source, Harwell Science and Innovations Campus, Didcot, Oxfordshire OX11 0DE, UK
[f] Savannah River Ecology Laboratory, University of Georgia, Aiken, SC 29808, USA
[g] Swiss Light Source, Paul Scherrer Institute, Villigen CH-5232, Switzerland

HIGHLIGHTS

- UO_2 and UO_3 particle reactivity examined in Savannah River Site lysimeter systems.
- Particles (placed in discrete 1 cm horizons) reacted for 1 year in SRS sediments.
- UO_2 readily oxidized / altered under vadose zone conditions.
- UO_3 readily altered, but U movement (both particle types) was limited to several cm.
- In SRS sediments, secondary U phases and sorption limit U migration in effluents.

GRAPHICAL ABSTRACT

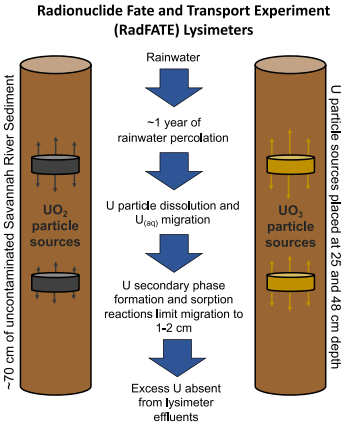

ARTICLE INFO

Editor: Daniel Alessi

Keywords:
Uranium
X-ray absorption spectroscopy
Speciation
Groundwater
Surface water

ABSTRACT

Uranium dioxide (UO_2) and metaschoepite ($UO_3 \cdot nH_2O$) particles have been identified as contaminants at nuclear sites. Understanding their behavior and impact is crucial for safe management of radioactively contaminated land and to fully understand U biogeochemistry. The Savannah River Site (SRS) (South Carolina, USA), is one such contaminated site, following historical releases of U-containing wastes to the vadose zone. Here, we present an insight into the behavior of these two particle types under dynamic conditions representative of the SRS, using field lysimeters (15 cm D x 72 cm L). Discrete horizons containing the different particle types were placed at two depths in each lysimeter (25 cm and 50 cm) and exposed to ambient rainfall for 1 year, with an aim of understanding the impact of dynamic, shallow subsurface conditions on U particle behavior and U migration. The dissolution and migration of U from the particle sources and the speciation of U throughout the lysimeters was assessed after 1 year using a combination of sediment digests, sequential extractions, and bulk and μ-focus X-ray spectroscopy. In the UO_2 lysimeter, oxidative

* Corresponding author.
E-mail address: gareth.law@helsinki.fi (G.T.W. Law).

http://dx.doi.org/10.1016/j.scitotenv.2022.160862
Received 29 August 2022; Received in revised form 25 November 2022; Accepted 7 December 2022
Available online 12 December 2022

dissolution of UO_2 and subsequent migration of U was observed over 1–2 cm in the direction of waterflow and against it. Sequential extractions of the UO_2 sources suggest they were significantly altered over 1 year. The metaschoepite particles also showed significant dissolution with marginally enhanced U migration (several cm) from the sources. However, in both particle systems the released U was quantitively retained in sediment as a range of different U(IV) and U(VI) phases, and no detectable U was measured in the lysimeter effluent. The study provides a useful insight into U particle behavior in representative, real-world conditions relevant to the SRS, and highlights limited U migration from particle sources due to secondary reactions with vadose zone sediments over 1 year.

1. Introduction

Uranium (U) has been released to the environment through civil nuclear and defense related activities worldwide. Sources of contamination include U mining, waste effluent discharges, weapons testing/fallout, and nuclear accidents (Salbu et al., 2003; Lind et al., 2007; McDonald, 2011; Falck, 2015; Imoto et al., 2017; Ochiai et al., 2018). Uranium is a redox-active, radio- and chemo-toxic element, and it is potentially mobile in the environment. Its environmental prevalence and the long half-life of uranium's major isotopes, ^{238}U (4.468×10^9 y) and ^{235}U (7.038×10^8 y), make it a key risk-driver in radioactive contaminated land management and the long-term storage of U nuclear wastes (Morris et al., 2011). As such, understanding U migration and fate in the geosphere is critical.

Uranium is the most common contaminant radionuclide at US Department of Energy (DOE) sites (Riley et al., 1992). The Savannah River Site (SRS), which is the subject of this study, is a DOE site that functioned as a nuclear fuel fabrication facility in US atomic weapons program (Evans et al., 1992). At present, the site is used for materials storage and legacy waste processing, with significant remediation now underway (Chang et al., 2014; Kaplan et al., 2011). Uranium contamination at SRS is well documented, with the most significant releases occurring in the 1950s (Evans et al., 1992). An estimated 43 tons of depleted and natural U have been released into the Tims Branch watershed at SRS, accounting for ~97 % of the site's gross (environmental) alpha activity (DOE, 1990; Kaplan et al., 2020; Parker et al., 2022).

Uranium's environmental mobility is largely determined by its speciation relative to local physico- chemical conditions. In oxidizing or near-surface conditions, U(VI) persists as the uranyl cation (UO_2^{2+}), which can readily form soluble carbonate complexes in solution when the pH >5 (Grenthe et al., 2011; Brookshaw et al., 2015). Under reducing conditions, sparingly soluble U(IV)-phases dominate, which include uraninite (UO_2) and non-crystalline U(IV) products (Newsome et al., 2014). Indeed, U(IV) solids are generally regarded as an environmentally favorable species for remediation efforts and both abiotic and biotic reduction pathways have been proposed as viable options for the environmental immobilization of U (Lovley et al., 1991; Lloyd and Renshaw, 2005; Cherkouk et al., 2016). Abiotic U(VI) reduction can occur following sorption of U on reactive mineral surfaces, such as Fe-/Mn-(oxy)hydroxides (Jeon et al., 2005). The incorporation of U into neoforming mineral phases is also possible and has recently been shown to be a successful mechanism for the stabilization of U(V) (Pidchenko et al., 2017; Roberts et al., 2017), which can be produced via microbial reduction (Renshaw et al., 2005; Vettese et al., 2020).

Many studies examining U behavior in the geosphere have focused on the remediation of soluble U(VI) phases. However, particulate U is also present at many nuclear sites in various chemical forms, including U-metal phases and U-oxides of varying stoichiometry (e.g., UO_2, UO_3, and U_3O_8) (IAEA, 2011; Ochiai et al., 2018; Salbu, 2008; Bower et al., 2019). Intact UO_2 particles have been isolated from numerous contaminated sites, often originating from nuclear fuel material (e.g., Kashparov et al., 2019; Ochiai et al., 2018). Although UO_2 particles have been shown to persist in the environment for many years (Oughton and Kashparov, 2007), oxidative dissolution and subsequent migration of U through the geosphere is possible, with UO_2 forming secondary U(VI) phases, such as metaschoepite (UO_3•nH2O), under oxidizing conditions (Buck et al., 2004a; Finch and Ewing, 1992). Indeed, the production of metaschoepite colloids from UO_2 powders (44–105 μm) has also been reported following exposure to aerated deionized water, and aged metallic depleted uranium munitions are known to form metaschoepite as a major corrosion product (Buck et al., 2004b; Handley-Sidhu et al., 2009; Wang et al., 2016).

At SRS, U has been released in the form of dissolved salts and particulate material, including U metal fragments. Any U metal fragments are now assumed to have oxidized to form poorly soluble compounds at the site (e.g., U_3O_8, UO_2; Evans et al., 1992). Whilst particulate U material can represent a significant fraction of the overall U inventory at SRS and other contaminated sites, little is known about the long-term stability of U particles in the subsurface or how they affect the overall geochemistry of U in the environment. Further environmentally relevant studies are required.

Unlike fully saturated, flowing column systems or batch-type laboratory studies, field lysimeters permit examination of the effects of vadose-zone conditions in contaminated sediments (Abdou and Flury, 2004). Exposed to rainfall and other ambient conditions, lysimeters simulate an environment representative of the shallow subsurface, complete with a variable hydrologic cycle. Given the expected prevalence of multi-valence U solids in the shallow subsurface at contaminated sites, and the high concentrations of U (including particulates) released to the vadose zone at SRS, the objective of this study was to examine the dissolution and mobility of U from two contrasting types of U particles (ceramic UO_2 and metaschoepite (UO_3•nH_2O)) under conditions representative of the SRS vadose zone. Accordingly, field lysimeter experiments containing SRS sediment and discrete sources of ceramic UO_2 and metaschoepite particles were deployed for 12 months. Each lysimeter contained two source horizons, allowing assessment of particulate U behavior at varying depths in the sediment profile. Upon completion of the experiments, sediments from the lysimeters were examined using autoradiography, μ-XRF mapping, U L_{III}-edge μ-XANES, and bulk EXAFS to track U migration and speciation. Traditional geochemical analyses were also performed to assess U partitioning in the sediment.

2. Materials and methods

2.1. Uranium oxide sources

All experiments were subject to radiological risk assessment. A commercial, synthetic, ceramic UO_{2+x} (where $x < 0.1$) (STREM Chemicals) and natural metaschoepite powder (UO_3●$n$$H_2O$) (where $n < 2$) (as per Bower et al., 2019) were used as U particle sources in the lysimeter experiments. The UO_2 and metaschoepite were ground lightly by hand in an agate mortar and pestle, then sieved (between 10 and 50 μm meshes). The UO_2 was then acid washed (4 % HNO_3) under O_2 free conditions, rinsed with deoxygenated, deionized (DI) H_2O, and finally dried under O_2 free N_2. The metaschoepite required no further washing (as per Bower et al., 2019). These operations were completed in a fumehood and FFP1 masks were worn as an extra precaution. The two particle sources were predominantly comprised of sub-micron crystallites that formed electrostatically bound clusters (in the case of the UO_2 source, some larger macro-crystals were also present) (see Supporting Information (SI) section 1 and Figs. S1 and S2). The uranium sources are herein termed 'UO_2' and 'UO_3' for brevity. The UO_2 was chemically pure (based on SEM-EDX and XRD measurements; SI section 1). Bower et al. (2019) has shown that the UO_3 source contains minor studtite (UO_4•4H_2O) (SI Fig. S2). Bulk XANES data of the unreacted UO_2 and metaschoepite stocks are also shown in SI Fig. S1.

Four uranium-containing sources were created with the above materials for emplacement in the lysimeters (2 x UO_2 and 2 x UO_3). There was ~3500 mg/kg U in each source. These sources were created by mixing an appropriate amount of UO_2 or UO_3 powder into 115 g of sediment (see below), and the U particle containing sediment was then moistened through addition of DI H_2O and molded into a cylinder (10 cm diameter, 1 cm depth; Fig. S3) for emplacement into the lysimeters during packing (see below).

2.2. Field Lysimeter design and set-up

Lysimeters were constructed according to an established method (Kaplan et al., 2018; Kilgo, 2018; Peruski et al., 2018; Roberts et al., 2012) at the Radionuclide Fate and Transport Experiment (RadFATE) facility at Clemson University (South Carolina, USA). Briefly, the setup utilized a 15 cm diameter PVC pipe that was ~72 cm in length. The bases of the pipes were fitted with a polypropylene grid covered with nylon mesh to allow water drainage. This base section was also encased in a PVC reducer (15 cm to 5 cm) and a barbed fitting housed in a 5 cm diameter bushing, which connected to flexible tubing to permit effluent collection. To ensure radiological safety, the 15-cm diameter PVC cores were placed within 20-cm diameter PVC secondary containment, which in turn were surrounded with a concrete backfill. The configuration is described in more detail in the SI (section 2, Fig. S4).

Two identical lysimeters (one for each U particle type) were packed with West Borrow Pit sediment from an uncontaminated area within the SRS. This sediment is a sandy clay loam representative of the vadose zone at the site. The clay fraction of this sediment (< 2 μm) contains kaolinite (> 95 %), Fe-oxyhydroxides (<2 % goethite and hematite) and quartz (< 2 %), with minor 2:1 clay phases (< 3 %, primarily as illite) (Montgomery et al., 2017). The sediment pH was 4.76. For more detailed characterization of the sediment see the SI, section 3 (Tables S1 and S2). The sediment was sieved (1 mm mesh) before packing and large pieces of organic matter were removed. The organic matter content of the sediment is 0.9 % after sieving (Montgomery et al., 2017). Duplicate sources of either UO_2 and UO_3 (see section 2.1) were placed horizontally at 25 cm and 48 cm from the top of each lysimeter and are herein termed the 'upper source' and 'lower source' for each particle type, respectively. The diameter of the sources was 10 cm and each source was placed in the (horizontal) centre of the 15 cm PVC pipe (i.e., there was ~2.5 cm of non U-labelled sediment between the sources and the lysimeter tube wall). The lysimeters were packed with the sediment in increments of 5 cm by manually 'tapping' the core with the sediment on a concrete base (10 times) so that the sediment settled evenly. This procedure was used for packing the sediment below, between, and above the two uranium sources in each lysimeter.

The lysimeters were then fit with three soil moisture sensors (5TE, METER Group, Inc.) (at 25 cm, 34 cm, and 48 cm from the lysimeter top); the positions are detailed in Fig. S4. The probes were inserted horizontally and extended into the sediment from the pipe walls (~5 cm). Measurements were collected from the probes at two-hour intervals for the duration of the experiment. The probes were used to determine the dielectric permittivity, bulk electrical conductivity (dS/m), and temperature (°C). The dielectric permittivity was then used to calculate the volumetric water content (VWC) using a calibration equation previously determined for the SRS sediment (Kilgo, 2018; Fig. S5). The lysimeters were left open to the environment for 12 months between May 2017 to May 2018, during which time approximately 128 cm of precipitation fell, which is comparable to the yearly mean rainfall of 122 cm precipitation near the SRS (SRR, 2020).

2.3. Lysimeter sampling

Drainage effluent from the lysimeters was collected in acid cleaned high-density polyethylene (HDPE) bottles that were periodically sampled six times during the 12-month experiment. Changes in effluent pH were recorded using a semi-micro pH electrode (Thermo Scientific 8115BN ROSSTM). Effluent samples were acidified (2 % HNO_3) and shaken before measuring the concentration of Fe, Mg, Ca, K, and U using inductively coupled plasma mass spectrometry (ICP-MS, Thermo Scientific X-series 2).

After 12 months, the lysimeters were capped and removed from the test bed and transferred to a HEPA-filtered glove box that contained O_2 free Ar. After removal of the probes and drainage system, the PVC lysimeter encasings were cut in half lengthwise (along the longitudinal axis, i.e., the direction of water flow) and a thin stainless-steel sheet was inserted between the two halves of the lysimeter to reveal intact cross-sections of the reacted sediment. An intact sub-section of sediment was extracted from each of the original U source horizons using a rectangular aluminum cutter (10 × 7 × 2 cm) (see SI, Fig. S3). The sediment block was carefully lifted out of the bulk sediment and immediately flash frozen in liquid N_2 to preserve the sediment. Wire mesh was put over the top and bottom surfaces to stabilize the sediment structure and allow fluid exchange through the blocks during later resin embedding. The remaining sediment in each lysimeter was sectioned in ~1 cm increments, homogenized, and placed in sterile polyethylene bags flushed with Ar. Of note, during sectioning of the UO_2 lysimeter, the sectioning resolution meant that the source was spread across two 1 cm sediment sections. After sectioning, the sediment fractions and preserved block sections were stored at −80 °C before further work.

Using an established method designed to maintain the redox-state and texture of the sediments at the point of sampling (Jilbert et al., 2008; Bower et al., 2019), the preserved blocks were embedded in SpurrTM low viscosity epoxy resin. The resin-embedded blocks were then cut lengthwise (along the water flow direction) across the original U source horizon using a diamond saw. Polished 'thin' (100 μm) sections were created from the exposed surfaces and mounted on optical grade quartz slides for autoradiography and μ-focus X-ray analysis.

2.4. Sediment analysis

The elemental content of sediment samples reacted in the lysimeters was assessed by digesting 0.5 g of sediment in boiling *aqua regia* for 2 h followed by ICP-MS analysis (Agilent 7700×) (see SI section 4 for further detail). Aqua regia (3:1, HCl:HNO_3) has previously been shown to completely dissolve UO_2 fuel elements (2 h at ~100 °C) (Flanary et al., 1959). It has also been shown in soils to totally dissolve sulfates, phosphates, iron oxides, carbonates, and organically bound metals, and only partially digest silicate and aluminosilicate minerals (EPA, 1996). Sequential extractions were also performed using an adaptation of the Tessier extraction (Tessier et al., 1979). Sequential extractions are designed to selectively extract contaminants that are associated with operationally defined fractions of a soil / sediment system being studied. The resulting data are qualitative and should not be over interpretated, as shown for U in past work (e.g., Kaplan and Serkiz, 2001). In the current work, 0.5 g of sediment was leached using chemical extractants of increasing strength. The targeted extraction phases and reagents were: "exchangeable" (0.1 M $MgCl_2$); "carbonate-associated / weak-acid extractable" (0.11 M CH_3COOH); "reducible" (0.5 M NH_2OH•HCl); "oxidizable" (8.8 M H_2O_2 and 1 M $NH_4CH_3CO_2$); and "residual" (aqua regia 3:1). The extractions were carried out under a normal laboratory atmosphere and further information on the extraction of these phases can be found in the SI (Table S3). Further, the UO_2 stock material used in the lysimeter experiments (mixed with sediment, but not reacted), went through the same extraction protocol. The UO_3 stock was completely used during set-up of the lysimeter experiment and was thus not extracted in the same way.

2.5. Autoradiography

Autoradiography was used to assess the distribution of radioactivity across the resin-embedded thin sections. Sections were exposed to a storage phosphor screen for 72 h and images were collected using a Typhoon™ 9410 variable mode imager with 50 μm resolution. The thin sections were also analyzed using BeaQuant™ real-time digital autoradiography. Here, the slides were carbon coated and cleaned with compressed air to remove any dust. Data was collected for alpha emitting radionuclides by

tuning the amplification gain of the BeaQuant™. Exposure times ranged between 24 and 120 h. The BeaQuant had a spatial resolution of ~30 μm.

2.6. Bulk XAS and μXAS and XRF

Bulk U L_{III} edge XANES and EXAFS data from discrete sediment sections were collected on beamline B18 at the Diamond Light Source, UK. Data was collected in fluorescence mode at 78 K using a 36 element Ge detector. An in-line Y-foil was used for energy calibration. All X-ray absorption spectroscopy (XAS) spectra were aligned, normalized, and background corrected using ATHENA (Demeter Package) (Ravel and Newville, 2005). Linear combination fitting of the XANES region was performed using ATHENA to assess the relative contributions of U(IV) and U(VI) to the sample spectra, using standards from the ACREDAS database (of UO_2 and $U(VI)_{aq}$) (Opel et al., 2007). An error of ±10 % is assumed for the linear combination fitting method (Kelly et al., 2008). EXAFS fitting was performed using model scattering paths from ACREDAS standards in ARTEMIS (Demeter Package) (Hellenbrandt, 2004; Ravel and Newville, 2005). For the EXAFS fitting, the Debye-Waller factor and interatomic distance were refined for each path, and the degeneracy of each path was optimized by manually varying the value and comparing the fits. The addition of each shell in the EXAFS fit was evaluated using an F-test (Downward et al., 2007).

μ-focus X-ray fluorescence (μ-XRF) mapping and μ-XANES data were collected on the MicroXAS beamline (X05-LA) at the Swiss Light Source. Possible beam-induced damage from the focused X-rays was evaluated (see Fig. S5). The μ-XRF maps were collected at 17600 eV with a horizontal beam size of either ~25 μm or 1 μm. The dwell time on the sample per point was 0.1 s, and as such XRF mapping did not result in beam induced speciation changes (Fig. S6). The U L_{III}-edge XANES spectra were collected using a defocused beam (~25 μm) to also mitigate against beam induced changes. A KETEK GmbH silicon drift detector (SDD) was used, and energy calibration was performed using a Y-foil. The μ-XRF images and scatter plots were created using PyMCA software. The μ-XANES were processed using the same method as for bulk XANES.

3. Results and discussion

3.1. Geochemical probes

Breakthrough of rainwater for the two lysimeters occurred between 75 and 85 days. The effluent pH in both systems varied over the duration of the experiment between 4.5 and 5.5 (Fig. S7). Rainfall pH in Clemson, SC, is ~5.5. The saturated VWC of the sandy clay loam used in this work was nearly 47 %. Over the first 14-days of the experiment, the sediment remained relatively dry in both lysimeters, with a VWC <15 % (Fig. S8). The VWC then steadily increased over time at all depths from the initially dry state of the soil and then remained between 15 % to 35 % with fluctuations based on rainfall (Fig. S8). For more details on the geochemical probe data see the SI (Section 6.2).

3.2. Effluents and sediment geochemistry

The concentrations of Na, K, Ca, Mg, Fe, and U in the lysimeter drainage effluents over time are shown in Fig. S9. U remained below 1 μg/L throughout. Background uranium concentrations in uncontaminated SRS groundwaters are ~1 μg/L (Evans et al., 1992) and the EPA Maximum Contaminant Level (MCL) for drinking water is 30 μg/L. No overall U loss was thus recorded from the lysimeters over 1 year. The concentrations of exchangeable cations (Na, K, Mg, Ca) steadily decreased over the duration of the experiment. Interestingly, increased effluent Fe was measured at comparable time points from both lysimeters; however, there was variability in concentrations between the two systems. In the UO_2 lysimeter, elevated Fe concentrations (50–100 μg/L) were observed between 275 and 331 days. In the UO_3 lysimeter, periodic spikes of Fe were observed, with ~1000 μg/L in solution after 168 days, and ~ 1360 μg/L released after 331 days. The release of Fe into solution from both lysimeters likely indicates the occurrence of microbially mediated Fe(III)-reduction in parts of the SRS sediment lysimeters. Sediments from the SRS site are known to contain Fe-reducing bacteria which can promote metal reduction, including U(VI) reduction and stabilization (Scala et al., 2006; Li et al., 2014). Whether redox stratification occurred in the lysimeters with depth from the surface, or in micro-environments is unknown.

Sediment major element concentration profiles (Fig. 1) show the distribution of U throughout the UO_2 and UO_3 lysimeters and thereby the extent of U migration following dissolution of the upper and lower sources (with and against rainwater flow direction). During the sectioning routine, a significant fraction of each U source was removed as intact sections for resin embedding and μ-focus characterization (Fig. S3B). As such, the acid extraction data for the remaining, homogenized sediments can only be used to indicate the extent of U migration, rather than provide accurate mass balance.

In the UO_2 lysimeter system, U migration occurred, with U present in sediments ~2 cm above and up to ~3 cm below both sources, although we note during sectioning that the upper UO_2 source was spread over two 1 cm samples in our sampling regime (see Section 2.3). In the UO_3 systems,

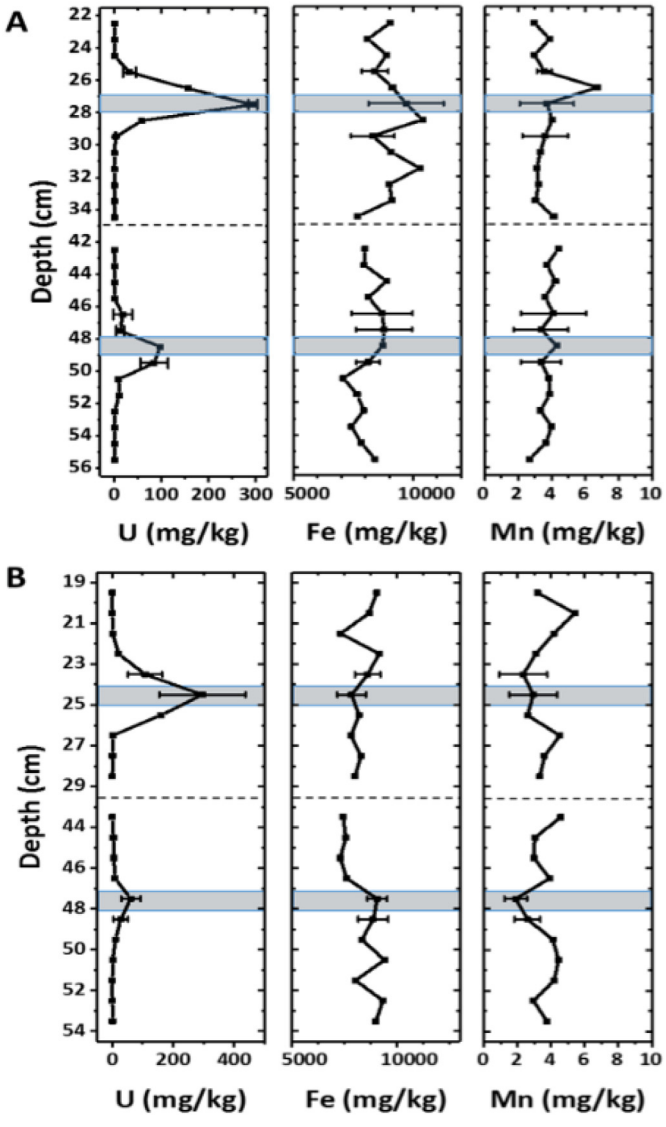

Fig. 1. U, Fe, and Mn concentrations with depth for the (A) UO_2, and (B) UO_3 systems after 12 months of reaction. Digestion data (black line) were acquired through aqua regia digests of the sediment sections (taken in ~1 cm increments). The approximate locations of the particle sources are indicated by the blue boxes. The dashed lines represent a break in the sediment profile. Errors indicate the standard deviation (1σ) of triplicate extractions performed on select samples.

elevated U concentrations were evident ~3 cm above and up to ~4 cm below the source horizons (albeit this was more marked for the upper source horizon; Fig. 1B). Previous work with the same UO_3 source material in saturated flow-through column experiments conducted with sediment representative of the UK Sellafield site, has shown that these UO_3 particles completely dissolve within 6–12 months under both oxic and reducing groundwater conditions (Bower et al., 2019). In that work, some of the released U became associated with the sediment over a distance of >5 cm, whilst a significant amount was released in the column effluents (including as U-colloids). In the current study, UO_3 derived effluent U was not observed (Fig. S9); instead, U was retained within 5 cm of the original source location (Fig. 1B). However, it is important to note that comparisons cannot be easily made between the experiments due to the use of different sediment types, saturated vs. vadose zone conditions, flow length etc. No discernible trends in sediment Fe and Mn concentrations were evident after 1 year of reaction (Fig. 1A).

3.3. Sequential extractions

Sequential extraction data for each source horizon and the surrounding sediments (taken 1–2 cm above and below the sources) are shown in Fig. 2. The extractions were carried out under a normal laboratory atmosphere. As with the *aqua regia* sediment digestions, the sequential extractions were performed on sediments after removal of a significant fraction of the UO_2 and UO_3 sources. Uranium concentrations per sediment section are therefore not comparable; as a result, we discuss the percentage of U extracted per step, normalized to the total U extracted per sediment section. This provides a qualitative indication of how U partitioned in the solids during alteration/weathering of the particle sources.

The UO_2 source material underwent the same sequential extraction procedure immediately after being mixed with SRS sediment. Here, the majority of the U was extracted in the residual (*aqua regia*) step (82 ± 3 %), with the balance distributed reasonably evenly between the other extraction steps (approximately 6 %, 6 %, 3 %, and 2 % respectively, in the exchangeable ($MgCl_2$), carbonate / weak acid extractable (acetic acid), reducible ($NH_2OH{\cdot}HCl$), and oxidizable (H_2O_2 then $NH_4CH_3CO_2$) steps). Sequential extraction of material from the two "upper source" samples (see Section 2.3), and the lower source sample, after 1 year of reaction, showed that only ~28–31 % of U was now extracted in the residual step. Further, the carbonate step now accounted for a significant proportion of extractable U (~23–29 %), and higher proportions on U were also extracted in the other steps (Fig. 2). Samples then taken from 1 cm above and 1–2 cm

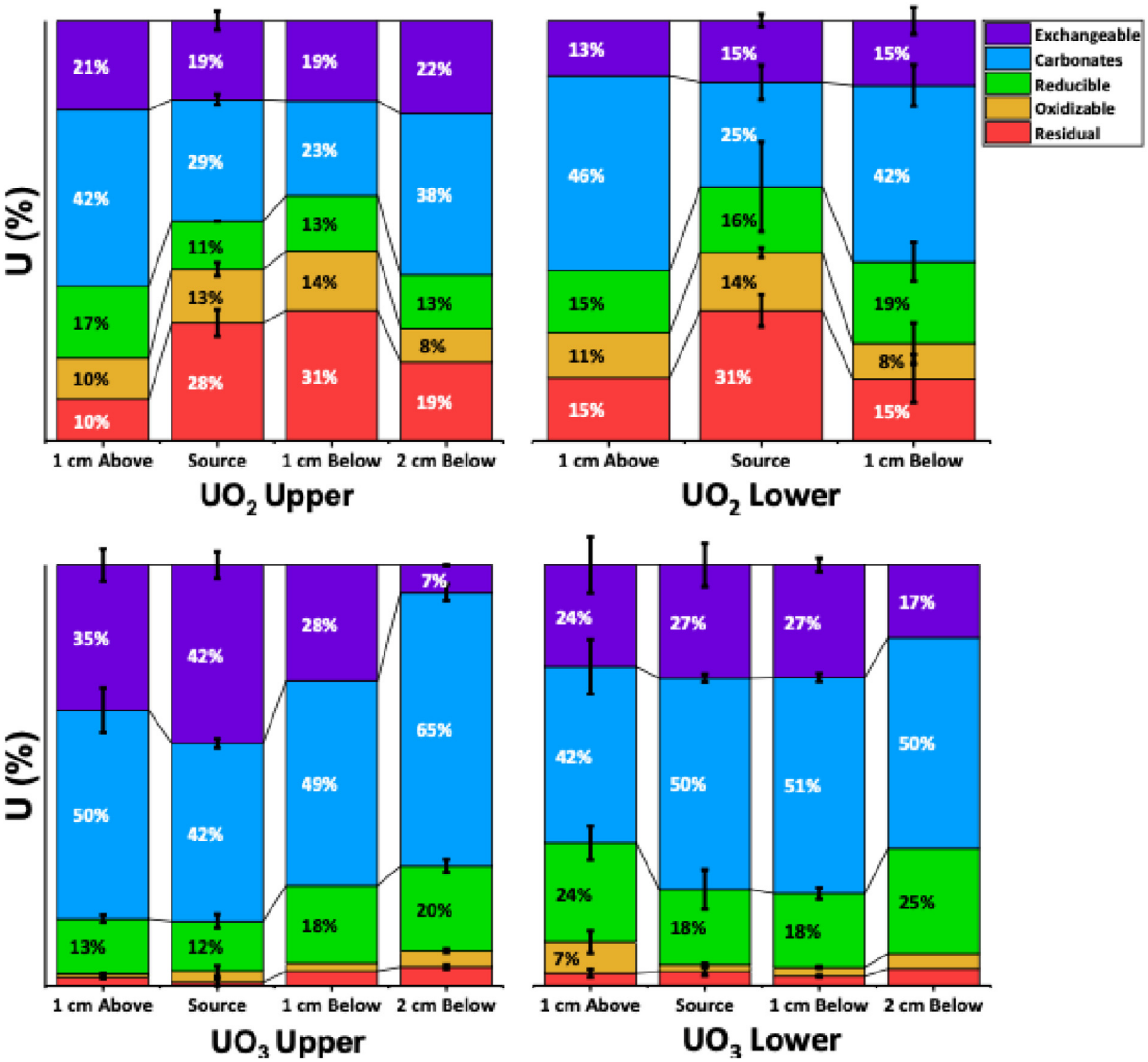

Fig. 2. Sequential extraction results for the UO_2 and UO_3 lysimeters, where the concentration of uranium in each extraction step is given as a percentage of the total extracted U (summed across all reagents). Sediments were collected from 1-cm thick sample layers located 1 cm above, 1 cm below, 2 cm below, and at the source. Errors indicate the standard deviation (1σ) of triplicate measurements. Extractions yielding <5 % are not labelled with a value.

below the UO_2 sources released ~15–20 % more U in the carbonate step, with a commensurate decrease of U in the residual step (Fig. 2).

The high proportion of "residual" U remaining in the UO_2 source samples after 1 year likely reflects remaining UO_2 particles. Further, whilst the UO_2 labelled sediment horizons were carefully placed in the lysimeter, we cannot rule out possible mixing or other physical transport of added UO_2 particles into the surrounding sediment, which may explain the presence of U in the residual fractions immediately above and below the source horizons. In contrast, the U released with the exchangeable, carbonate / weak acid extractable, and reducible steps likely indicates the extraction of sediment associated U (e.g., U associated with carbonates, Fe-(oxyhydr)oxides etc.), following oxidative dissolution of UO_2 and migration of released U into the surrounding matrix. Comparable transport of Np, due to oxidative dissolution of NpO_2, was observed in lysimeter experiments with the same sediment (Peruski et al., 2018). However, it may also possible that the U was extracted from the surface of corroded UO_2 grains that have moved out of the original source horizon. Uranium extracted during the "oxidizable" step could represent U associated with organic material (e.g., Fuller et al., 2020); however, this cannot be assessed independently from oxidative remobilization of U(IV) phases (either from the source material, or in combination with sediment associated U(IV)) using these reagents (Flanary et al., 1959) and we note that the organic content of the SRS sediment was low. Regardless of the specific mineral associations, a significant amount of the UO_2 source material had been altered during 1 year of reaction, creating a range of more labile U phases. The speciation of the U in these sediments was further investigated using XAS (see Section 3.4).

Within the UO_3 lysimeter source horizons after 1 year of reaction, the majority of the extractable U was released in the exchangeable (27–42 %) and carbonate extractions steps (42–50 %) (Fig. 2). In turn, 12–18 % of the extractable U was released in the reducible step, with minor quantities of the total U (<7 %) released in the oxidizable and residual steps. Uranium partitioning above and below the source horizons was broadly comparable, although there was a marginal increase (~10–20 %) in the U extracted in the carbonate / weak acid extractable and reducible steps, and a commensurate decrease in exchangeable U in the direction of water flow. Overall, the extraction data indicates that the UO_3 particles altered/dissolved and then the remobilized U became bound to a range of phases, which, like the U released from UO_2 dissolution, could reflect U complexation with carbonates, Fe-(oxyhydr)oxides, organics etc. in the sediment. However, the shift from exchangeable U to that extracted with the carbonate / weak acid extractable and reducible steps may reflect that U released from the source horizons gradually forms more stable inner sphere complexes with reactive mineral surfaces (as per Bower et al., 2019). This was further investigated using XAS.

3.4. Bulk X-ray absorption spectroscopy

Bulk U L_{III}-edge XANES and EXAFS spectra were collected from a select number of sediment samples from both lysimeters (Fig. 3). The results of linear combination fitting of the XANES using UO_2 and $U(VI)_{aq}$ end members are shown in Fig. S10. The results of the EXAFS modelling are provided in Table S5.

For the UO_2 lysimeter, three sediment sections were examined by bulk XAS: the upper source horizon (labelled A in Fig. 3-I), 1 cm below the upper source (B), and the lower source horizon (C). Again, as noted in the previous section, and as manifest in the extraction data, part of the upper source was likely sampled across two 1 cm sections. Linear combination fitting of the upper source horizon XANES (Fig. S10) gave a 37 % contribution from U(VI) to the spectrum, indicating that there was significant oxidation of the UO_2 over 1 year of reaction in this part of the lysimeter. Under strongly oxidizing conditions, UO_2 dissolution can occur rapidly (hours–days), resulting in formation and liberation of U(VI) from the UO_2 surface (Bi et al., 2013). It is also possible that this U(VI) remains as an oxidized surface layer on the UO_2 particles, as the liberation of U(VI) will be dependent on the concentration of complexing ligands (e.g., carbonate, calcium) and dissolved oxygen (Bi and Hayes, 2014). In the sample taken 1 cm below the source horizon, the XANES was modelled with a higher U(VI) component (75 %), indicating that whilst U(IV) was present, U(VI) is likely being transported away from the UO_2 source to then sorb to the sediment, which limits further U migration. In contrast, the lower UO_2 source XANES was modelled with a 95 % contribution from U(IV). As indicated by the effluent Fe data, the lysimeters likely supported anaerobic processes such as microbially-mediated Fe(III)-reduction. As O_2 supply comes from the top of the lysimeters (via gas diffusion and percolation of rainwater through the sediment), reducing conditions are more likely to be supported deeper in the lysimeters, which remained saturated for most of the experiment (Fig. S8). The contrasting XANES between the two UO_2 source horizons may indicate that the lower horizon was being altered under anaerobic conditions. However, as detailed by μ-focus XAS analysis (see Section 3.5), this is not clear. As such, there was likely marked heterogeneity in UO_2 oxidation deeper in the lysimeter that could not be identified by the bulk-sampling.

The EXAFS data collected from bulk samples taken from both UO_2 source horizons was initially modelled using a uraninite structure. However, reflecting the XANES, fitting of this sample was improved by addition of an axial O backscattering contribution at 1.78 ± 0.02 Å (CN = 0.85) (Fig. 3-I, spectrum A; Table S5). This U–O_{axial} distance is typical of a uranyl-like O coordination (Thompson et al., 1997), confirming that some of the U in the source region had oxidized to U(VI). The model fit for this spectrum was optimized with 7 equatorial O at 2.36 ± 0.01 Å. There are typically 8 O atoms in the first co-ordination shell (~2.36 Å) of a U(IV)-oxide species. A U—U backscattering contribution could also be modelled at 3.87 ± 0.01 Å for the upper UO_2 source (Table S5), suggesting that a reasonable amount of crystalline UO_2 remained within the original source horizon. However, the low co-ordination number (CN = 6) of this U—U pair-correlation suggests the presence of nanoparticulate UO_2 (i.e., the starting material) or reprecipitated, nano-crystalline U(IV) (Brookshaw et al., 2015; Bhattacharyya et al., 2017).

EXAFS data collected from the sediment sampled 1 cm below the upper UO_2 source (Fig. 3, spectrum B) was best modelled using a uranyl-like coordination in accordance with the higher U(VI) contribution (75 %) to the XANES. Here, 1.5 axial oxygens were best fit at 1.80 ± 0.01 Å. Uranyl is expected to have 2 axial oxygen atoms at 1.8 Å and six equatorial oxygens at 2.42 Å (Shi et al., 2018). The model for this sample was improved with six equatorial oxygen atoms at 2.39 ± 0.01 Å; however, there remains a significant contribution (25 %) from U(IV) as indicated by the XANES and axial oxygen occupancy (Fig. 3-I). Despite this, no evidence for a U—U path (~3.80 Å) was present in the Fourier transform of the EXAFS data (Fig. 3, spectrum B). The lack of a U—U backscattering feature in this spectrum would indicate that the U(IV) in this sediment section is not predominantly present as crystalline UO_2 and instead may be non-crystalline U(IV). Non-crystalline U(IV), a common bio-reduced endmember, does not display a U—U backscatter contribution owing to the loss of medium range order (Alessi et al., 2012). In view of past work showing U inner sphere sorption to Fe–minerals, further fits with Fe were also attempted (e.g., Bargar et al., 1999; Moyes et al., 2000; Sylwester et al., 2000; Wang et al., 2013). Whilst the inclusion of a Fe backscattering shell in the model (at 3.54 ± 0.07 Å) did give a 78 % improvement in the fit, its inclusion was not statistically relevant.

In agreement with XANES linear combination fitting, EXAFS modelling of the lower UO_2 source horizon (spectrum C) indicated that crystalline UO_2 remained the dominant species in this sample, with seven equatorial O backscatters present at 2.35 ± 0.01 Å, and eight U backscatters at 3.86 ± 0.01 Å. As per the upper UO_2 source, the occupancy of the U backscatter shell is lower than expected for uraninite (12 U at ~3.85 Å) (Brookshaw et al., 2015). This was the only sample analyzed in this region of the lysimeter; however, bulk sediment digests indicate that U was liberated from the original source horizon and that it had migrated from the source, both in the direction of flow and via upward diffusion. As discussed for the XANES data from this sample, the bulk data may not reflect the heterogeneity present around the lower UO_2 source horizon. The anoxic corrosion of UO_2 has been reported in environmentally relevant synthetic

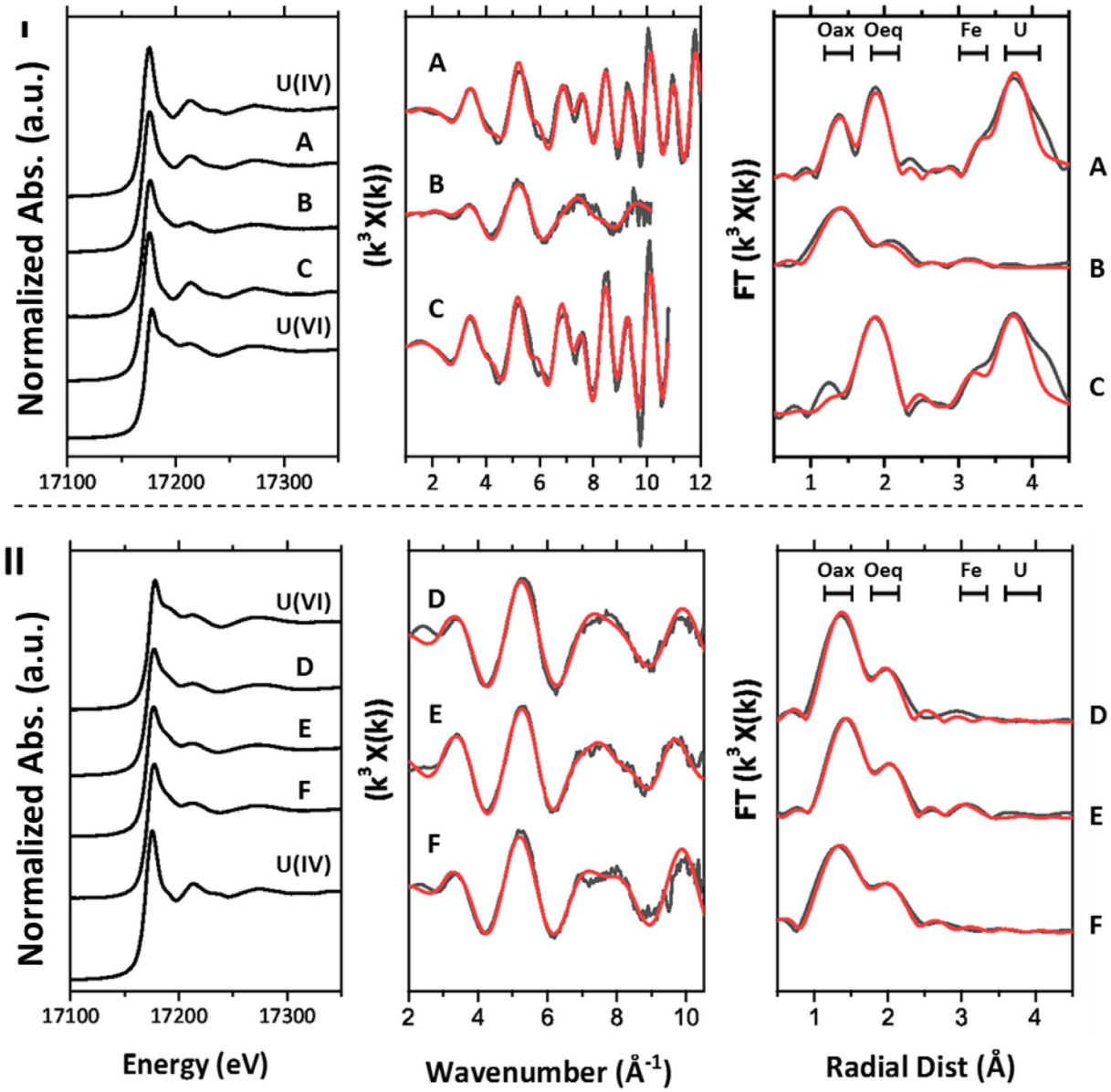

Fig. 3. Bulk U L_{III}-edge XANES and k^3-weighted EXAFS data (black lines) from: (I) the UO_2 lysimeter, and (II) UO_3 lysimeter. Spectra from the UO_2 system are: (A) upper source horizon; (B) 1 cm below the upper source; (C) lower source horizon. For the UO_3 system: (D) upper source horizon; (E) 1 cm above upper source horizon; and (F) lower source horizon. The red lines indicate the best-fit models as detailed in Table S5. FT = the non-phase shifted Fourier transform of the EXAFS data. Areas marked O_{ax}, O_{eq}, Fe, and U in the FT show the expected peak positions for these back-scatterers (non-phase corrected).

groundwaters (Cera et al., 2000), and uraninite has been shown to undergo extensive dissolution in natural environments (Janeczek and Ewing, 1992).

Three sediment sections from the UO_3 system were also analyzed using bulk U L_{III}-edge XAS: the upper source horizon (spectrum D, Fig. 3-II), 1 cm above the upper source (E), and the lower source horizon (F). Linear combination fitting of the XANES from these horizons indicates partial reduction of the initial U(VI) to U(IV), with spectra D, E, and F showing U(IV) contributions of 22 %, 25 %, and 17 %, respectively (Fig. S10). A uranyl-like co-ordination could be modelled from the EXAFS data for all spectra (Fig. 3-II and Table S5), with split equatorial O occupancy consistent with uranyl-oxide hydrates (i.e., schoepite and metaschoepite) (Pidchenko et al., 2017). Spectrum D, collected from within the upper UO_3 source horizon was best fit with 1.6 axial O backscatters at 1.78 ± 0.01 Å, and 6 equatorial O between 2.25 and 2.42 Å. The addition of an Fe scattering path (CN = 1.0) at 3.47 ± 0.02 Å also yielded a 92 % improvement in the fit. The presence of an Fe- backscattering shell in the EXAFS may again indicate U surface complexation with Fe-(oxy)hydroxide minerals, as has been previously observed in dynamic environmental systems (Kaplan et al., 2016; Bower et al., 2019). Data from the lower UO_3 source (spectrum F) was best fit with 1.7 axial O backscatters at 1.80 ± 0.01 Å, reflecting the slightly higher U(VI) content in comparison to the upper source horizon (although this is within the error of the LCF method). Equatorial O refinement matched that of the upper UO_3 source, with six O backscatters modelled between 2.21 and 2.40 Å. Although the O coordination numbers were similar between the two UO_3 source horizons, the lower source contained a shoulder feature in the EXAFS at 7.3 $Å^{-1}$ (Fig. 3-II, spectrum F). This feature was not observed in the data from the upper UO_3 source and could not be accounted for with varied O co-ordination or the addition of common U bonding paths (C, Fe) to the fit.

The greatest proportion of U(IV) (25 %) was apparent in spectrum E (1 cm above the upper UO_3 source), represented by a significantly reduced axial O contribution (1.5 O atoms at 1.80 ± 0.01). The equatorial shells were modelled with four O atoms at 2.27 ± 0.01 Å and three O atoms at 2.45 ± 0.01 Å. The higher occupancy in the equatorial O shell may reflect

an increased O contribution from U(IV) phases in this spectrum (Shi et al., 2018). As with the upper UO_3 source, spectrum E was successfully fit with one Fe atom (3.51 ± 0.05 Å), further indicating U associations with mineral surfaces; however, this Fe scatterer only provided a 90 % improvement in the fit.

The capacity for U(VI) reduction in the sediment system (up to 25 % U (IV)), particularly in the upper source, was an interesting finding, especially given that the UO_2 emplaced in the parallel lysimeter at a similar depth, underwent significant oxidation. This phenomenon may be a result of the formation of micro-environments in the sediment, with pockets of anoxia or ingress of oxygenated rainwater creating non-uniform redox profiles with depth.

3.5. High resolution autoradiography and μ-focus XRF and XANES

3.5.1. UO_2 lysimeter system

Autoradiography images from the resin-embedded thin-sections reveal the distribution of radioactivity across the two UO_2 source regions after 12 months of reaction (Fig. 4, panel I). The radioactivity within the two UO_2 source horizons is relatively concentrated suggesting that, consistent with extraction data and bulk XAS (Figs. 2 and 3), a significant proportion of the U remained in the vicinity of the source region, likely as partly altered UO_2 particles and/or secondary U products. However, some diffuse radioactivity was present outside of the source horizons, indicating some UO_2 dissolution, U-transport, and subsequent U-complexation by the SRS sediment. Coarse (30 μm horizontal beam) XRF maps collected within the upper UO_2 source horizon showed the presence of small (<10 μm) U hotspots within the sediment, and these are likely to be added UO_2 particles (Fig. 4-II, map 1). The μ-XRF map taken from the lower boundary of this UO_2 source (Fig. 4-II, map 2) showed a more diffuse U distribution along the direction of water flow, which likely represents a fraction of liberated U that has subsequently bound to the sediment matrix. Higher resolution (1 μm horizontal beam) μ-XRF mapping within and outside of this region (Fig. 4-III, maps 1* and 2*) revealed these trends in more detail, with concentrated U hot-spots, likely from intact crystalline UO_2 particles of variable size, and low concentrations of more diffuse U evident (i.e., not associated with crystalline particles). This mixture of concentrated and dispersed U is consistent with the bulk XAS data, suggesting the presence of both U(IV) (i.e., intact UO_2) and U(VI) from oxidative alteration.

Discrete areas within and outside the UO_2 source horizons were also selected for μ-XANES analysis. μ-focus XANES from μ-XRF maps within the upper UO_2 source horizon revealed significant variability in U speciation at the μm-scale. Spectrum G (Fig. 4-IV), collected from a concentrated hot-spot (<20 μm) at the center of the source horizon (Fig. 4-III, map 1*), was 95 % U(IV) (Fig. S10). Down-flow, towards the region of more diffuse U, significant point-to-point variability in U speciation was observed. Linear combination fitting suggested a 20 % U(VI) contribution to μ-XANES

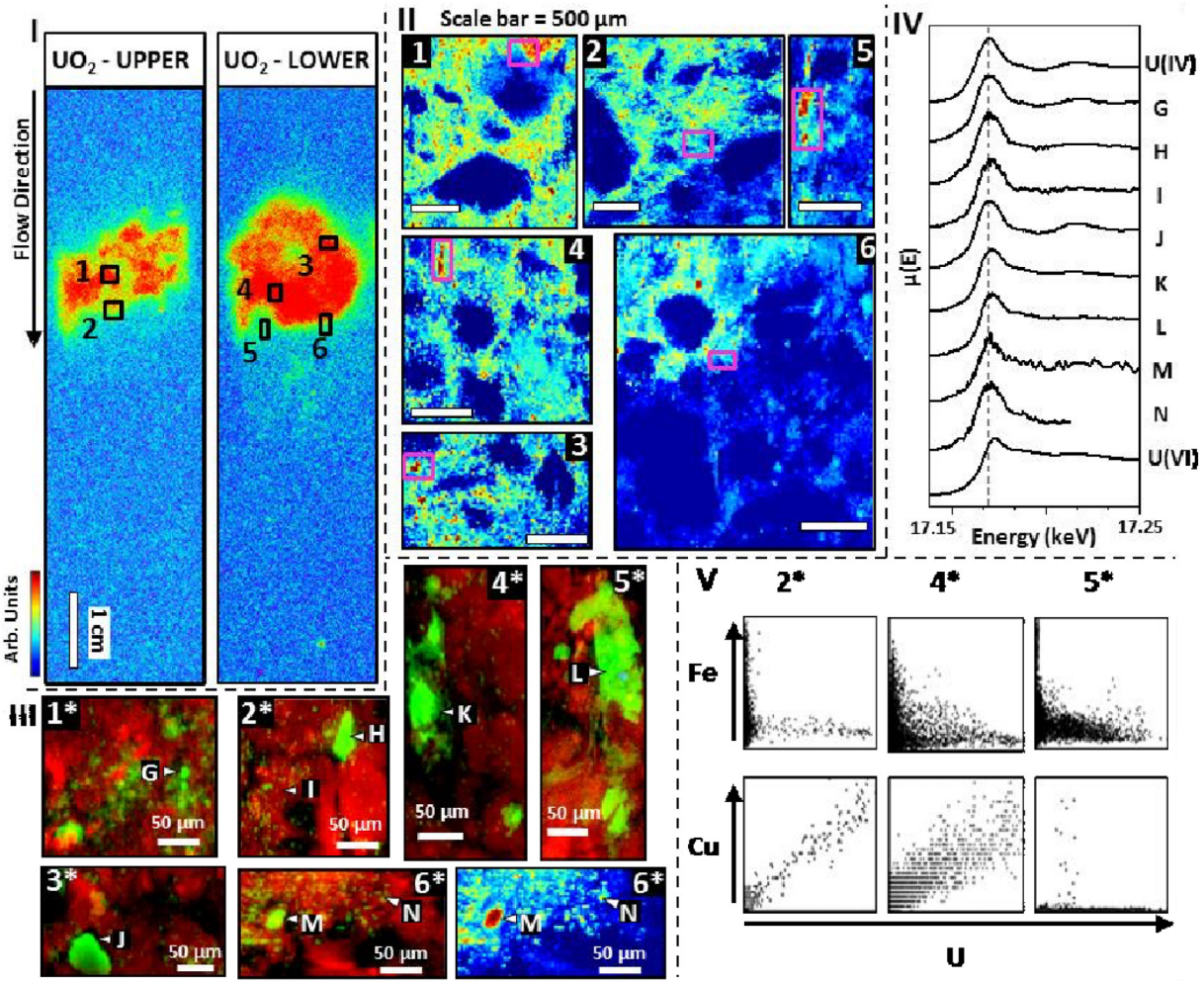

Fig. 4. (I) Autoradiography images of the thin sections taken from upper and lower source zones of the UO_2 lysimeter. The areas mapped for defocused μ-XRF images are indicated by black boxes. (II) The μ-XRF maps (defocused beam) showing the distribution of uranium. Areas chosen for high resolution μ-XRF mapping are indicated by pink boxes. (III) The composite images (red = Fe, green = U) taken from the high resolution μ-XRF maps, with white triangles indicating the positions chosen for μ-XANES analysis. (IV) The μ-focus XANES spectra (G–N) from the UO_2 lysimeter, and standards for U(IV) and U(VI). (V) Correlation plots taken from the μ-XRF images.

from one hotspot (Fig. 4-IV, spectrum I), whilst another area (within 150 μm) was 97 % U(IV) (Fig. 4-IV, spectrum H).

Autoradiography imaging across the lower UO_2 source thin-section revealed a much more heterogenous U distribution in the sediment (~3 cm below the source boundary) compared to the upper UO_2 source (Fig. 4-I). Here, μ-XRF mapping showed a high proportion of (presumably) UO_2 particles in the source zone (Fig. 4-II, maps 3 and 4), however a much more prominent "wash" of liberated U was evident across the boundary of the source horizon (Fig. 4, Maps 5 and 6). Variable U oxidation states were also observed between U-rich areas within the lower source. In areas with high quantities of UO_2 particles, the U remained as U(IV) (95 %) (Fig. 4, spectrum J), which is consistent with the bulk XAS data (Fig. 3, spectrum C). However, towards the lower boundary of the source, U was relatively more oxidized. Spectra K and L, collected from the most diffuse regions of U, yielded the highest contributions from U(VI), at 61 % and 41 % respectively (Fig. 4-IV). As with the sediment digests and the bulk XAS data of the lower UO_2 source, the mixed speciation in this area suggests that liberated U has been carried out of the source horizon in migrating rainwater and binds to the sediment as U(IV) and U(VI), leaving behind residual UO_2.

At the region of highest U(VI) in the lower UO_2 source (Fig. 4-III, map 5*), μ-XRF mapping revealed a "plume" of U along the flow direction. Elemental correlation plots from this area indicate U association with sediment matrix elements (e.g., Fe, Cu) (Fig. 4-V). Despite indications of an Fe backscatterer in the bulk XAS of U(VI) from the UO_2 system (Fig. 3, spectrum B), the scatter plots from the thin sections do not indicate a strong correlation between U and Fe in the sediment. However, given the redox variability within these sediments and the small sample volume of the thin sections, it is likely that the bulk XAS better identifies the major trends in the local co-ordination chemistry of these heterogeneous environments. The mixed valence states of U in this area could suggest preferential flow paths through the UO_2 lysimeter, allowing oxygenated rainwater to pass through different areas of the sediments, creating a heterogeneous redox front. Preferential flow paths have been reported in other lysimeters at the sister facility at Savannah River Site (RadFLEX) (Peruski et al., 2017) and are expected to occur in the environment as a result of near-surface heterogeneity, cracks, and local surface depressions (Arora et al., 2019).

Interestingly, one area containing oxidized U(VI) (Fig. 4-III, map 4*) displayed a correlation between U and Cu, which could indicate U sorption to organic material (Bower et al., 2019). Although the organic matter content of the SRS sediment is low in this study (< 1 %), U (as both U(VI) and U (IV)) has a high adsorption affinity for organic matter (Mikutta et al., 2016; Bone et al., 2017; Fuller et al., 2020). Previously, the retardation of U(VI) in SRS sediment has been shown to be promoted by the presence of Fe-rich plaques on the roots of wetland plants (Chang et al., 2014). This immobilization is encouraged by favorable conditions for Fe reducing bacteria, which facilitate the reduction of U(VI) to U(IV), and provide potential sorption sites (Chang et al., 2014). The binding of U to organic phases has also been described following U particle dissolution experiments, evidenced by μ-XRF mapping, indicating U associations with Cu and Zn, which are common life supporting nutrients (Bower et al., 2019). U has also been found as

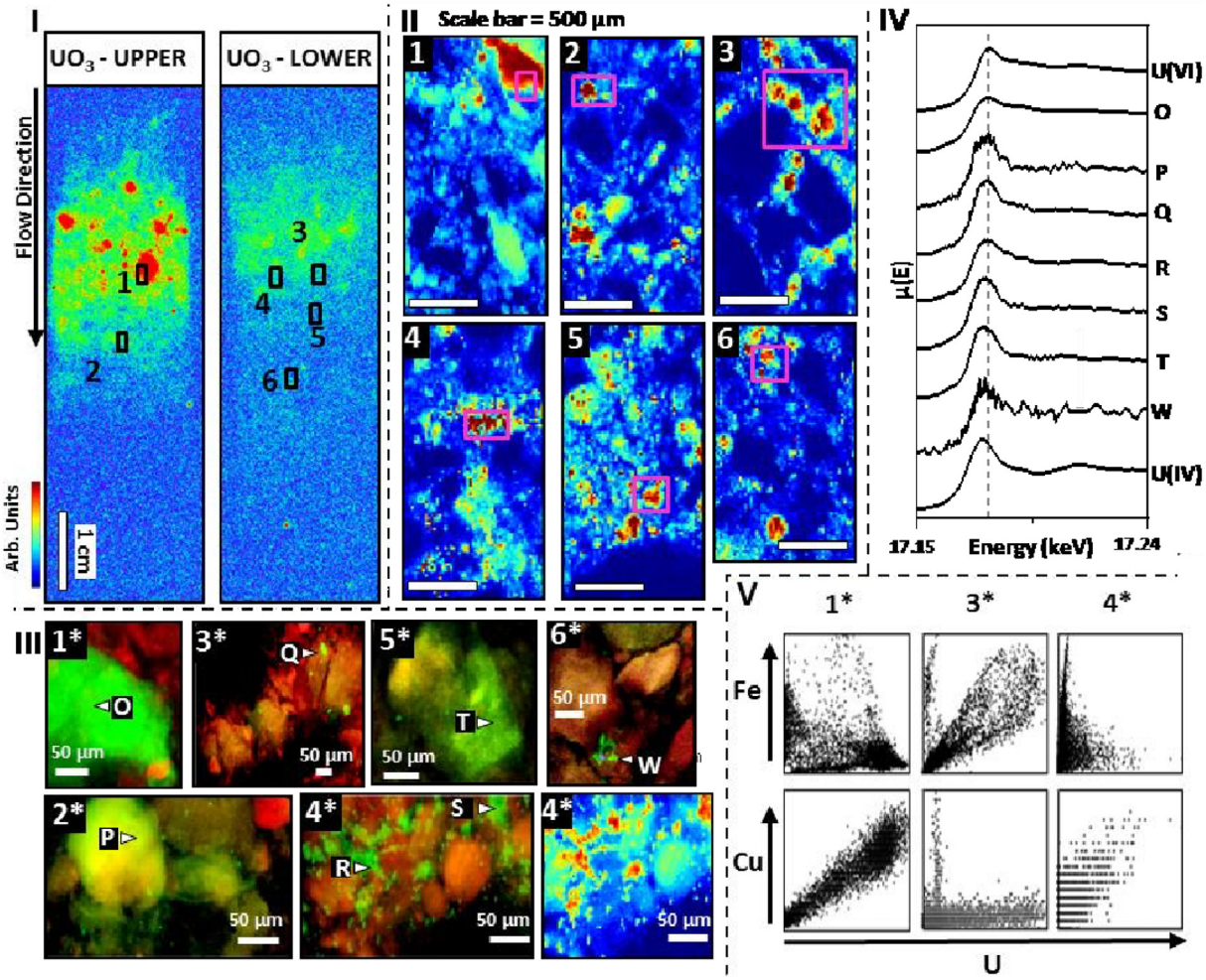

Fig. 5. (I) Autoradiography images of the upper and lower source horizons from the UO_3 system. The areas mapped for defocused μ-XRF imaging are indicated with black boxes. (II) The defocused μ-XRF maps showing the distribution of uranium. Key areas mapped with a focused beam are indicated by pink boxes. (III) The RGB images (red = Fe, green = U, blue = Cu) of the focused μ-XRF images. The areas chosen for μ-XANES analysis are indicated by white triangles and the corresponding letters (O—W). (IV) The μ-focus XANES spectra from the UO_3 thin sections and two standards for U(IV) and U(VI). (V) Correlation plots taken from the μ-XRF images.

a precipitate with Cu as metatorbernite [$CuUO_2PO_4$)-$8H_2O$] in the vadose zone beneath a contaminated area of the Hanford Site, USA (Catalano et al., 2006; Zachara et al., 2007). However, bulk EXAFS data from this system did not indicate scattering contributions from C (at ~2.91 Å), which is a known feature in the EXAFS signal of U bound to biomass (Kaplan et al., 2016). This would suggest that the binding of U(VI) to organic matter is not a dominant mechanism in this system.

3.5.2. UO_3 lysimeter system

Extensive dissolution of the UO_3 sources occurred. Autoradiography images from the UO_3 thin sections (Fig. 5-I) revealed a cm-scale, diffuse distribution of radioactivity across both source horizons in agreement with the U profile from sediment digests (Fig. 1). Small, concentrated hotspots of U were also visible within the original source area.

μ-focus XRF mapping within the upper UO_3 source region revealed a broad, heterogeneous distribution of U bound to mineral clasts but also dispersed through the sediment matrix. Unlike the UO_2 system, the more diffuse distribution of U is indicative of near complete dissolution of the source material and subsequent binding of solubilized U to reactive surfaces. A similar distribution of U sourced from UO_3 dissolution was observed by Bower et al. (2019) under both oxic and anoxic conditions. Bower et al. (2019) also reported a positive correlation between dissolved U and Fe in XRF mapping of their sediment. In the SRS UO_3 system, U released from both source horizons into the surrounding sediment was strongly correlated with Fe and Cu, indicative of possible U-binding to Fe-bearing mineral surfaces and organic matter, respectively (Fig. 5-V). Analysis of μ-XANES data collected from a U rich region in the upper source showed the U was 89 % U(VI) (Fig. 5-IV, spectrum O). In contrast, the region directly below this source (in the direction of rainwater flow) contained 84 % U(IV) (Fig. 5-IV; spectrum P). As such, there was marked heterogeneity in U speciation in the upper source over small spatial scales.

In the lower UO_3 source, hot spots of radioactivity in autoradiography images were fewer and less intense (Fig. 5-I). Two small (<500 μm) hot spots were identified ~5 cm down-flow from the original source horizon, suggesting that U had become associated with the sediment following migration. These areas were also imaged using high-resolution autoradiography (BeaQuant) (Fig. S11). μ-XANES taken from a hotspot within the lower UO_3 source suggests that the U here was 42 % U(IV) (Fig. 5-IV, spectrum Q), and, coincident with the trend from the upper UO_3 source, the μ-XRF data shows a correlation between U and Fe (Fig. 5-III; map 3*). The μ-XRF maps from the low U concentration, diffuse zone along the flow direction (Fig. 5, maps 5 and 6) show that U is present as both discrete, concentrated areas (~2 mm) and a dispersed "wash" through the sediment matrix. μ-XANES and linear combination fitting from within this zone revealed a mixture of oxidation states. Indeed, spectra R and S taken from within this region showed 47 % and 78 % U(IV) respectively (Fig. 5-IV). As per the upper UO_3 source, and combined with the bulk data from this lysimeter, there is marked heterogeneity in U distribution and speciation upon UO_3 dissolution in the SRS sediment, including creation of U(IV)-phases. Similar heterogeneity was also seen by Bower et al. (2019), with U(VI), non-crystalline U(IV), and UO_2 products identified in their sediment after UO_3 dissolution.

4. Implications

This work highlights the complexity of U particle behavior and U biogeochemistry in the environment under geochemically relevant, vadose zone conditions. Using field scale lysimeter experiments and spatially resolved analytical techniques, it is clear that U biogeochemistry varies significantly at the μm-scale. In both particle systems tested (UO_2 and UO_3), we show that whilst U is readily solubilized from the U particle sources, the migration of U species in water through the SRS sediment appears to be effectively limited by biotic / abiotic redox reactions, or U(VI/IV) complexation/sorption to reactive mineral surfaces. Therein, sediment Fe-phases and possibly, (to a lesser extent) organic matter, were implicated in U sequestration, as observed in other studies. These reactions, over 1 year and under vadose conditions, were sufficient to limit U migration to several cm. As such, U particle sources in vadose zone systems such as those at SRS, are unlikely to pose major U migration risks. This contrasts to behavior seen in saturated sediment systems (e.g., Bower et al., 2019), where at least for UO_3 particle sources, U-colloid production presents a possible U migration risk.

CRediT authorship contribution statement

Study conceptualization: CMF, GTWL, WRB, BAP, DK. Student supervision: GTWL, WRB, BAP, FRL, ICL, KM. Data collection, data processing, data interpretation: CMF, WRB, GTWL, KP, BAP, AEM, JFWM, SS, KM, DK, DG, PW, DFS, MSK. Manuscript writing: CMF, GTWL, WRB, FRL, BAP, and DK. Manuscript editing: All authors. Funding acquisition: GTWL, FRL, ICL, KM, SS, BAP, DK.

Data availability

Data will be made available on request.

Declaration of competing interest

The authors declare no competing interests.

Acknowledgements

This work was supported by a PhD bursary to CMF from AWE and the UK EPSRC Next Generation Nuclear Centre for Doctoral Training (EP/L015390/1). GL, FRL, ICL, and KM acknowledge funding from UK NERC grants NE/M014088/1 and NE/L000202/1. NE/L000202/1 is the NERC RATE programme which was co-funded by the UK Environment Agency and Radioactive Waste Management Ltd. GL also acknowledges funding from the Finnish KYT2022 programme. BP acknowledges support from the U.S. Department of Energy Office of Science (DOE-OS), Office of Basic Energy Sciences, and Office of Biological and Environmental Research under Award Number DE-SC-0012530. DK acknowledges DOE-OS funding from the Environmental Systems Science Program (DE-AC02-06CH11357) and DOE-Environmental Management funding through a Cooperative Agreement (DE-EM0005228) with The University of Georgia Research Foundation. We thank University of Manchester staff members Steve Stockley, Alistair Bewsher, Paul Lythgoe, and Dr. Heath Bagshaw, and University of Helsinki staff member Dr. Katie Doig for technical assistance and advice. Diamond Light Source and the Swiss Light Source are thanked for beamtimes SP 16611, SP16939, SP17243 and 20181008.

Appendix A. Supplementary data

The Supporting Information contains additional information on the U source materials, the lysimeters, the SRS sediment, experimental methods, and additional results. Supplementary data to this article can be found online at https://doi.org/10.1016/j.scitotenv.2022.160862

References

Abdou, H.M., Flury, M., 2004. Simulation of water flow and solute transport in free- drainage lysimeters and field soils with heterogeneous structures. Eur. J. Soil Sci. 55 (2), 229–241.
Alessi, D.S., Uster, B., Veeramani, H., Suvorova, E.I., Lezama-Pacheco, J.S., Stubbs, J.E., Bargar, J.R., et al., 2012. Quantitative separation of monomeric U(IV) from UO_2 in products of U(VI) reduction. Environ. Sci. Technol. 46 (11), 6150–6157.
Arora, B., Dwivedi, D., Faybishenko, B., Jana, R.B., Wainwright, H.M., 2019. Understanding and predicting vadose zone processes. Rev. Mineral. Geochem. 85 (1), 303–328.
Bargar, J.R., Reitmeyer, R., Davis, J.A., 1999. Spectroscopic confirmation of uranium(VI)-carbonato adsorption complexes on hematite. Environ. Sci. Technol. 33 (14), 2481–2484.
Bhattacharyya, A., Campbell, K.M., Kelly, S.D., Roebbert, Y., Weyer, S., Bernier-Latmani, R., Borch, T., 2017. Biogenic non-crystalline U(IV) revealed as major component in uranium ore deposits. Nat. Commun. 8 (1), 15538.
Bi, Y., Hayes, K.F., 2014. Surface passivation limited UO_2 oxidative dissolution in the presence of FeS. Environ. Sci. Technol. 48 (22), 13402–13411.

Bi, Y., Hyun, S.P., Kukkadapu, R., Hayes, K.F., 2013. Oxidative dissolution of UO_2 in a simulated groundwater containing synthetic nanocrystalline mackinawite. Geochim. Cosmochim. Acta 102, 175–190.

Bone, S.E., Dynes, J.J., Cliff, J., Bargar, J.R., 2017. Uranium(IV) adsorption by natural organic matter in anoxic sediments. Proc. Natl. Acad. Sci. U. S. A. 114 (4), 711–716.

Bower, W.R., Morris, K., Livens, F.R., Mosselmans, J.F.W., Fallon, C.M., Fuller, A.J., Natrajan, L., et al., 2019. Metaschoepite dissolution in sediment column systems— implications for uranium speciation and transport. Environ. Sci. Technol. 53 (16), 9915–9925.

Brookshaw, D.R., Pattrick, R.A.D., Bots, P., Law, G.T.W., Lloyd, J.R., Mosselmans, J.F.W., Vaughan, D.J., et al., 2015. Redox interactions of Tc(VII), U(VI), and Np(V) with microbially reduced biotite and chlorite. Environ. Sci. Technol. 49 (22), 13139–13148.

Buck, B.J., Brock, A.L., Johnson, W.H., Ulery, A.L., 2004a. Corrosion of depleted uranium in an arid environment: Soil-Geomorphology, SEM/EDS, XRD, and Electron Microprobe Analyses. Soil Sediment Contam. 13 (6), 545–561.

Buck, E.C., Mcnamara, B.K., Hanson, B.D., 2004b. Alternative Conceptual Model for Colloid Generation From Commercial Spent Nuclear Fuel. U.S. Department of Energy: Pacific Northwest National Laboratory, Washington, DC.

Catalano, J.G., McKinley, J.P., Zachara, J.M., Heald, S.M., Smith, S.C., Brown, G.E., 2006. Changes in uranium speciation through a depth sequence of contaminated Hanford sediments. Environ. Sci. Technol. 40 (8), 2517–2524.

Cera, E., Grivé, M., Bruno, J., Ollila, K., 2000. Modelling of the UO_2 Dissolution Mechanisms in Synthetic Groundwater. POSIVA 2000-10., Posiva Oy., Helsinki.

Chang, H.-S., Buettner, S.W., Seaman, J.C., Jaffé, P.R., Koster van Groos, P.G., Li, D., Peacock, A.D., Scheckel, K.G., Kaplan, D.I., 2014. Uranium immobilization in an iron- rich rhizosphere of a native wetland plant from the Savannah River Site under reducing conditions. Environ. Sci. Technol. 48 (16), 9270–9278.

Cherkouk, A., Law, G.T.W., Rizoulis, A., Law, K.A., Renshaw, J.C., Morris, K., Livens, F.R., Lloyd, J.R., 2016. Influence of riboflavin on the reduction of radionuclides by Shewanella oneidenis MR-1. Dalton Trans. 45, 5050-5037.

DOE (US), 1990. Continued Operation of K-, L- and P-Reactors Savannah River Site, Aiken, South Carolina. Vol. I. U.S. Department of Energy, Washington, DC available at: https://www.energy.gov/sites/prod/files/2015/07/f25/EIS-0147-FEIS-Vol1.pdf (accessed 14 June 2019).

Downward, L., Booth, C.H., Lukens, W.W., Bridges, F., 2007. A variation of the F-test for determining statistical relevance of particular parameters in EXAFS fits. AIP Conference Proceedings. 882, pp. 129–131.

EPA (US), 1996. Method 3050B: Acid Digestion of Sediments, Sludges, and Soils, Revision 2. Washington, DC.

Evans, A.G., Bauer, L.R., Haselow, J.S., Hayes, D.W., Martin, H.L., McDowell, W.L., Pickett, J.B., 1992. Uranium in the Savannah River Site Environment, Westinghouse Savannah River Company WSRC-RP-92-315, Aiken, SC.

Falck, W.E., 2015. Radioactive and other environmental contamination from uranium mining and milling. Environmental Remediation and Restoration of Contaminated Nuclear and Norm Sites. Elsevier Inc., pp. 3–34.

Finch, R.J., Ewing, R.C., 1992. The corrosion of uraninite under oxidizing conditions. J. Nucl. Mater. North-Holland 190 (C), 133–156.

Flanary, J.R., Clark, W.E., Goode, J.H., Kibbey, A.H., 1959. Development of the sulfex process for decladding stainless-steel-clad power reactor fuel elements with fulfuric acid. Oak Ridge National Laboratory, Tennessee.

Fuller, A.J., Leary, P., Gray, N.D., Davies, H.S., Mosselmans, J.F.W., Cox, F., Robinson, C.H., Pittman, J.K., McCann, C.M., Muir, M., Graham, M.C., Utsunomiya, S., Bower, W.R., Morris, K., Shaw, S., Bots, P., Livens, F.R., Law, G.T.W., 2020. Organic complexation of U(VI) in reducing soils at a natural analogue site: Implications for uranium transport. Chemosphere 254, 126859.

Grenthe, I., Drożdżyński, J., Fujino, T., Buck, E.C., Albrecht-Schmitt, T.E., Wolf, S.F., 2011. Uranium. In: Morss, L.R., Edelstein, N.M., Fuger, J. (Eds.), The Chemistry of the Actinide and Transactinide Elements. Springer Netherlands, Dordrecht, pp. 253–698.

Handley-Sidhu, S., Worsfold, P.J., Livens, F.R., Vaughan, D.J., Lloyd, J.R., Boothman, C., Sajih, M., et al., 2009. Biogeochemical controls on the corrosion of depleted uranium alloy in subsurface soils. Environ. Sci. Technol. 43 (16), 6177–6182.

Hellenbrandt, M., 2004. The Inorganic Crystal Structure Database (ICSD)-Present and Future. Crystallogr. Rev. 10 (1), 17–22.

IAEA, 2011. Radioactive particles in the environment: Sources, particle characterization and analytical techniques. International Atomic Energy Agency (IAEA), Vienna.

Imoto, J., Ochiai, A., Furuki, G., Suetake, M., Ikehara, R., Horie, K., Takehara, M., Yamasaki, S., Nanba, K., Ohnuki, T., Law, G.T.W., Grambow, B., Ewing, R.C., Utsunomiya, S., 2017. Isotopic signature and nano-texture of cesium-rich micro-particles: Release of uranium and fission products from the Fukushima Daiichi Nuclear Power Plant. Sci. Rep. 7, 5409.

Janeczek, J., Ewing, R.C., 1992. Dissolution and alteration of uraninite under reducing conditions. J. Nucl. Mater. 190 (c), 157–173.

Jeon, B.H., Dempsey, B.A., Burgos, W.D., Barnett, M.O., Roden, E.E., 2005. Chemical reduction of U(VI) by Fe(II) at the solid-water interface using natural and synthetic Fe(III) oxides. Environ. Sci. Technol. 39 (15), 5642–5649.

Jilbert, T., de Lange, G., Reichart, G.-J., 2008. Fluid displacive resin embedding of laminated sediments: preserving trace metals for high-resolution paleoclimate investigations. Limnol. Oceanogr. Methods 6, 16–22.

Kaplan, D.I., Serkiz, S.M., 2001. Quantification of thorium and uranium sorption to contaminated sediments. J. Radioanal. Nucl. Chem. 248 (3), 529–535.

Kaplan, D.I., Roberts, K.A., Schwehr, K.A., Lilley, M.S., Brinkmeyer, R., Denham, M.E., Diprete, D., et al., 2011. Evaluation of a radioiodine plume increasing in concentration at the Savannah river site. Environ. Sci. Technol. 45 (2), 489–495.

Kaplan, D.I., Kukkadapu, R., Seaman, J.C., Arey, B.W., Dohnalkova, A.C., Buettner, S., Li, D., et al., 2016. Iron mineralogy and uranium-binding environment in the rhizosphere of a wetland soil. Sci. Total Environ. 569–570, 53–64.

Kaplan, D.I., Powell, B.A., Barber, K.K., DeVol, T.A., Dixon, K.L., Erdmann, B.J., Maloubier, M., et al., 2018. Radionuclide Field Lysimeter Experiment (RadFLEx). Geochemical and Hydrological Data for SRS Performance Assessments, Rep. No. SRNL-SRI-2017-00677. Savannah River National Laboratory, Aiken, SC.

Kaplan, D.I., Smith, R., Parker, C.J., Baker, M., Cabrera, T., Ferguson, B.O., Kemner, K.M., Laird, M., Logan, C., Lott, J., 2020. Uranium attenuated by a wetland 50 years after release into a stream. ACS Earth Space Chem. 4, 1360–1366.

Kashparov, V., Salbu, B., Levchuk, S., Protsak, V., Maloshtan, I., Simonucci, C., Courbet, C., et al., 2019. Environmental behavior of radioactive particles from chernobyl. J. Environ. Radioact. 208–209, 106025.

Kelly, S.D., Hesterberg, D., Ravel, B., 2008. Analysis of soils and minerals using x- ray absorption spectroscopy. Methods of Soil Analysis. Part 5. Mineralogical Methods. SSSA Book., Soil Science Society of America, Madison, WI, USA, pp. 387–464.

Kilgo, M.K., 2018. Environmental Impact Predictions for Disposal of Emerging Energy Technologies in Solid Waste Landfills: Application to Lithium Ion Batteries and Photovoltaic Modules, PhD dissertation 2409. Clemson University. https://tigerprints.clemson.edu/all_dissertations/2409.

Li, D., Seaman, J.C., Chang, H.-S., Jaffe, P.R., Koster van Groos, P., Jiang, D.-T., Chen, N., Lin, J., Arthur, Z., Pan, Y., Scheckel, K.G., Newville, M., Lanzirotti, A., Kaplan, D.I., 2014. Retention and chemical speciation of uranium in an oxidized wetland sediment from the Savannah River Site. J. Environ. Radioact. 131, 40–46.

Lind, O.C., Salbu, B., Janssens, K., Proost, K., García-León, M., García-Tenorio, R., 2007. Characterization of U/Pu particles originating from the nuclear weapon accidents at Palomares, Spain, 1966 and Thule, Greenland, 1968. Sci. Total Environ. 376 (1–3), 294–305.

Lloyd, J.R., Renshaw, J.C., 2005. Bioremediation of radioactive waste: radionuclide– microbe interactions in laboratory and field-scale studies. Curr. Opin. Biotechnol. 16 (3), 254–260.

Lovley, D.R., Phillips, E.J.P., Gorby, Y., a. and Landa, E.R., 1991. Microbial reduction of uranium. Nature 350 (6317), 413–416.

McDonald, P., 2011. Radioactivity in the Irish Sea. In: Warwick, P. (Ed.), Environmental Radiochemical Analysis IV. Royal Society of Chemistry, pp. 87–94.

Mikutta, C., Langner, P., Bargar, J.R., Kretzschmar, R., 2016. Tetra- and hexavalent uranium forms bidentate-mononuclear complexes with particulate organic matter in a naturally uranium-enriched peatland. Environ. Sci. Technol. 50 (19), 10465–10475.

Montgomery, D., Barber, K., Edayilam, N., Oqujiuba, K., Young, S., Biotidara, T., Gathers, A., et al., 2017. The influence of citrate and oxalate on ^{99}Tc(VII), Cs, Np(V) and U(VI) sorption to a Savannah River Site soil. J. Environ. Radioact. 172, 130–142.

Morris, K., Law, G.T.W., Bryan, N.D., 2011. Geodisposal of higher activity wastes. In: Harrison, R.M., Hester, R.E. (Eds.), Nuclear Power and the Environment, Issues in. Royal Society of Chemistry, Cambridge, UK, pp. 129–151.

Moyes, L.N., Parkman, R.H., Charnock, J.M., Vaughan, D.J., Livens, F.R., Hughes, C.R., Braithwaite, A., 2000. Uranium uptake from aqueous solution by interaction with goethite, lepidocrocite, muscovite, and mackinawite: an X-ray absorption spectroscopy study. Environ. Sci. Technol. 34 (6), 1062–1068.

Newsome, L., Morris, K., Lloyd, J.R., 2014. The biogeochemistry and bioremediation of uranium and other priority radionuclides. Chem. Geol. 363, 164–184.

Ochiai, A., Imoto, J., Suetake, M., Komiya, T., Furuki, G., Ikehara, R., Yamasaki, S., et al., 2018. Uranium dioxides and debris fragments released to the environment with cesium-rich microparticles from the Fukushima Daiichi Nuclear Power Plant. Environ. Sci. Technol. 52 (5), 2586–2594.

Opel, K., Weiß, S., Hübener, S., Zänker, H., Bernhard, G., 2007. Study of the solubility of amorphous and crystalline uranium dioxide by combined spectroscopic methods. Radiochim. Acta 95 (3), 143–149.

Oughton, D., Kashparov, V. (Eds.), 2007. Radioactive Particles in the Environment, NATO Science for Peace and Security Programme, 1st ed. Springer, Yalta.

Parker, C.J., Kaplan, D.I., Seaman, J.C., Powell, B.A., 2022. Uranium partitioning from contaminated wetland soil to aqueous and suspended iron-floc phases: Implications of dynamic hydrologic conditions on contaminant release. Geochim. Cosmochim. Acta 318, 292–304.

Peruski, K., Pope, R., Maloubier, M., Powell, B.A., 2017. Determination of Constituent Concentrations in Field Lysimeter Effluents, Anderson, SC. available at: https://www.nrc.gov/docs/ML1806/ML18067A486.pdf.

Peruski, K.M., Maloubier, M., Kaplan, D.I., Almond, P.M., Powell, B.A., 2018. Mobility of aqueous and colloidal neptunium species in field lysimeter experiments. Environ. Sci. Technol. 52 (4), 1963–1970.

Pidchenko, I., Kvashnina, K.O., Yokosawa, T., Finck, N., Bahl, S., Schild, D., Polly, R., Bohnert, E., Rossberg, A., Göttlicher, J., Dardenne, K., Rothe, J., Schäfer, T., Geckeis, H., Vitova, T., 2017. Uranium redox transformations after U(VI) coprecipitation with magnetite nanoparticles. Environ. Sci. Technol. 51 (4), 2217–2225.

Ravel, B., Newville, M., 2005. ATHENA, ARTEMIS, HEPHAESTUS: data analysis for x-ray absorption spectroscopy using IFEFFIT. J. Synchrotron Radiat. 12 (4), 537–541.

Renshaw, J.C., Butchins, L.J.C., Livens, F.R., May, I., Charnock, J.M., Lloyd, J.R., 2005. Bioreduction of uranium: environmental implications of a pentavalent intermediate. Environ. Sci. Technol. Am. Chem. Soc. 39 (15), 5657–5660.

Riley, R.G., Zachara, J.M., Wobber, F.J., 1992. Chemical contaminants on DOE lands and selection of contaminant mixtures for subsurface science research. US DOE Office of Energy Research. Subsurface Research Program, Washington DC, p. 77.

Roberts, K.A., Kaplan, D.I., Powell, B.A., Bagwell, L., Almond, P., Emerson, H., Hixon, A., et al., 2012. SRNL radionuclide field lysimeter experiment: baseline construction and implementation. available at: https://pdfs.semanticscholar.org/dd45/6824e5589a6711cadd49a2ae1aebe699658e.pdf.

Roberts, H.E., Morris, K., Law, G.T.W., Mosselmans, J.F.W., Bots, P., Kvashnina, K., Shaw, S., 2017. Uranium(V) incorporation mechanisms and stability in Fe(II)/Fe(III) (oxyhydr)Oxides. Environ. Sci. Technol. Lett. 4 (10), 421–426.

Salbu, B., 2008. Radioactive particles released from different nuclear sources: with focus on nuclear weapons tests. In: Salbu, B., Skipperud, L. (Eds.), Nuclear Risks in Central Asia. Springer Netherlands, Dordrecht, pp. 7–17.

Salbu, B., Janssens, K., Lind, O.C., Proost, K., Danesi, P.R., 2003. Oxidation states of uranium in DU particles from Kosovo. J. Environ. Radioact. 64 (2-3), 167–173.

Scala, D.J., Hacherl, E.L., Cowan, R., Young, L.Y., Kosson, D.S., 2006. Characterization of Fe (III)-reducing enrichment cultures and isolation of Fe(III)- reducing bacteria from the Savannah River site, South Carolina. Res. Microbiol. 157 (8), 772–783.

Shi, W.-Q., Yuan, L.-Y., Wang, C.-Z., Wang, L., Mei, L., Xiao, C.-L., Zhang, L., et al., 2018. Exploring actinide materials through synchrotron radiation techniques. In: Fan, C., Zhao, Z. (Eds.), Synchrotron Radiation in Materials Science: Light Sources, Techniques, and Applications. Wiley, Weinheim, Germany, pp. 389–509.

SRR, 2020. Performance Assessment for the Saltstone Disposal Facility at the Savannah River Site. Rep. No. SRR-CWDA-2019-00001, Rev.0. Savannah River Remediation LLC, Aiken, SC.

Sylwester, E.R., Hudson, E.A., Allen, P.G., 2000. The structure of uranium (VI) sorption complexes on silica, alumina, and montmorillonite. Geochim. Cosmochim. Acta 64 (14), 37–41.

Tessier, A., Campbell, P.G.C., Bisson, M., 1979. Sequential extraction procedure for the speciation of particulate trace metals. Anal. Chem. 51 (7), 844–851.

Thompson, H.A., Brown, G.E., Parks, G.A., 1997. XAFS spectroscopic study of uranyl coordination in solids and aqueous solution. Am. Mineral. 82 (5-6), 483–496.

Vettese, G.F., Morris, K., Natrajan, L.S., Shaw, S., Vitova, T., Galanzew,J., Jones, D.L., and Lloyd, J.L., (2020), "Multiple Lines of Evidence Identify U(V) as a Key Intermediate during U(VI) Reduction by Shewanella oneidensis MR1", Environ. Sci. Technol., vol. 54(4), pp 2268–2276.

Wang, Z., Lee, S.W., Catalano, J.G., Lezama-Pacheco, J.S., Bargar, J.R., Tebo, B.M., Giammar, D.E., 2013. Adsorption of uranium(VI) to manganese oxides: X-ray absorption spectroscopy and surface complexation modeling. Environ. Sci. Technol. 47 (2), 850–858.

Wang, Y., von Gunten, K., Bartova, B., Meisser, N., Astner, M., Burger, M., Bernier- Latmani, R., 2016. Products of in situ corrosion of depleted uranium ammunition in Bosnia and Herzegovina soils. Environ. Sci. Technol. 50 (22), 12266–12274.

Zachara, J.M., Brown, C.F., Christensen, J., Davis, J.A., Dresel, P.E., Liu, C., Kelly, S., McKinley, J.P., Serne, R.J., Um, W., 2007. A site wide perspective on uranium geochemistry at the Hanford site. Pacific Northwest National Laboratory (PNNL), Richland, WA.